ARTICLES
PUBLISHED ONLINE: 20 MARCH 2011 | DOI: 10.1038/NMAT2986
nature materials

Porphysome nanovesicles generated by porphyrin bilayers for use as multimodal biophotonic contrast agents

Jonathan F. Lovell[1,2], Cheng S. Jin[1,2], Elizabeth Huynh[2,3], Honglin Jin[2,3], Chulhong Kim[4], John L. Rubinstein[3,5], Warren C. W. Chan[1], Weiguo Cao[6], Lihong V. Wang[4] and Gang Zheng[1,2,3]*

Optically active nanomaterials promise to advance a range of biophotonic techniques through nanoscale optical effects and integration of multiple imaging and therapeutic modalities. Here, we report the development of porphysomes; nanovesicles formed from self-assembled porphyrin bilayers that generated large, tunable extinction coefficients, structure-dependent fluorescence self-quenching and unique photothermal and photoacoustic properties. Porphysomes enabled the sensitive visualization of lymphatic systems using photoacoustic tomography. Near-infrared fluorescence generation could be restored on dissociation, creating opportunities for low-background fluorescence imaging. As a result of their organic nature, porphysomes were enzymatically biodegradable and induced minimal acute toxicity in mice with intravenous doses of 1,000 mg kg^{-1}. In a similar manner to liposomes, the large aqueous core of porphysomes could be passively or actively loaded. Following systemic administration, porphysomes accumulated in tumours of xenograft-bearing mice and laser irradiation induced photothermal tumour ablation. The optical properties and biocompatibility of porphysomes demonstrate the multimodal potential of organic nanoparticles for biophotonic imaging and therapy.

Therapeutic and diagnostic techniques benefiting from components that efficiently absorb light include fluorescent and colorimetric detection[1,2], photothermal and photodynamic therapy[3–5], photoacoustic tomography (also known as optoacoustic tomography)[6–9], optical frequency domain imaging[10] and multimodal techniques[11], among others. As inorganic nanoparticles often interact strongly with light, they can be used as agents for these techniques. For instance, quantum dots are valuable fluorescent probes and have extinction coefficients in the range of 10^5–10^6 M^{-1}cm^{-1} (ref. 12). Gold nanoparticles are useful for colorimetric detection, photothermal and photoacoustic techniques owing to their much higher extinction coefficients, of the order of 10^9–10^{11} M^{-1}cm^{-1} (ref. 13). Despite recent progress[14], optically active inorganic nanoparticles have not yet achieved broad clinical implementation, possibly stemming from drug loading typically being limited to the nanoparticle surface and concerns regarding long-term safety[15–18]. In contrast, organic nanoparticles (including liposomes, lipoproteins, micelles, nanospheres and polymersomes) have found many human therapeutic applications as a result of robust biocompatibility and drug-delivery capacity[18]. However, as these organic nanoparticles generally do not intrinsically absorb light in the near-infrared region, they have been of limited use for biophotonics. Although supramolecular assemblies can be formed entirely by porphyrin conjugates, intensely light-absorbing organic small molecules, these constructs have not been thoroughly explored as biophotonic tools owing to a lack of stability, solubility or biological utility[19]. Here we introduce 'porphysomes'; organic nanoparticles self-assembled from phospholipid–porphyrin conjugates that exhibit liposome-like structure and loading capacity, high absorption of near-infrared light, structure-dependent fluorescence quenching and excellent biocompatibility, and show promise for diverse biophotonic applications.

Porphysomes were formed by supramolecular self-assembly. The porphysome subunits consisted of porphyrin–lipid conjugates generated by an acylation reaction between lysophosphatidylcholine and pyropheophorbide, a chlorophyll-derived porphyrin analogue. This hydrophobic chromophore was positioned in place of an alkyl side chain, maintaining an amphipathic structure (Fig. 1a). This conjugate could be self-assembled in aqueous buffer with extrusion to form porphysomes. A concentration of 5 molar% polyethylene glycol (PEG)–lipid was included in the formulation to enhance *in vivo* pharmacokinetics[20]. Transmission electron microscopy showed that these porphysomes were spherical vesicles of 100 nm in diameter (Fig. 1b). At higher magnifications, the porphysome structure was revealed as two layers of higher-density material separated by a 2 nm gap, corresponding to two separate monolayers of porphyrin. Pyropheophorbide porphysomes exhibited two absorption peaks, one at 400 nm and one in the near-infrared window at 680 nm (Fig. 1c). Further redshifted porphysomes (760 nm) were produced by using subunits generated from another type of porphyrin; a bacteriochlorophyll analogue that was synthesized in the same manner as pyropheophorbide–lipid. Alternatively, a protocol was developed to insert metal ions into the porphyrin–lipid structure, resulting in shifted optical density bands (440 nm and 670 nm) and demonstrating the unique phenomenon that porphysomes can form metal-chelating bilayers. These different

[1]Institute of Biomaterials and Biomedical Engineering, University of Toronto, Ontario M5G 1L7, Canada, [2]Ontario Cancer Institute, University Health Network, Ontario M5G 1L7, Canada, [3]Department of Medical Biophysics, University of Toronto, Ontario M5G 1L7, Canada, [4]Department of Biomedical Engineering, Optical Imaging Lab, Washington University in St Louis, Missouri 63130, USA, [5]Hospital for Sick Children Research Institute, Ontario M5G 1X8, Canada, [6]Department of Chemistry, Shanghai University, Shanghai 200444, China. *e-mail: gang.zheng@uhnres.utoronto.ca.

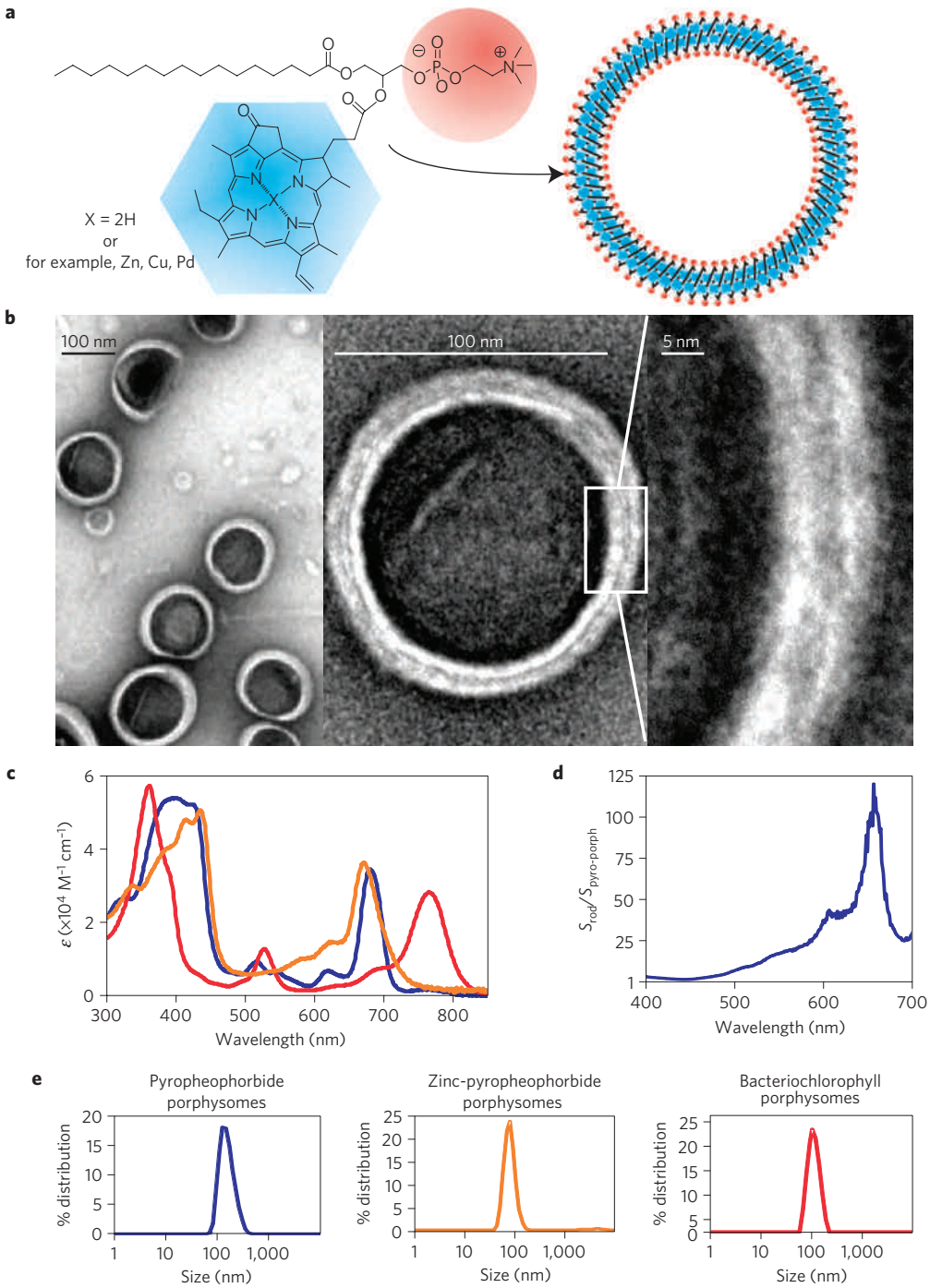

Figure 1 | Porphysomes are optically active nanovesicles formed from porphyrin bilayers. a, Schematic representation of a pyropheophorbide-lipid porphysome. The phospholipid headgroup (red) and porphyrin (blue) are highlighted in the subunit (left) and assembled nanovesicle (right). **b**, Electron micrographs of negatively stained porphysomes (5% PEG-lipid, 95% pyropheophorbide-lipid). **c**, Absorbance of the porphyrin-lipid subunits incorporated in porphysomes formed from pyropheophorbide (blue), zinc-pyropheophorbide (orange) and bacteriochlorophyll (red) in PBS. **d**, Resonance light scattering spectra ratio between gold nanorods and pyropheophorbide porphysomes. Nanorod and porphysome concentration was adjusted to have equal optical density at 680 nm. **e**, Dynamic light scattering size profiles of indicated porphysomes recorded in PBS.

types of porphysome could be useful in scenarios in which specific operating wavelengths are required (for example, to match a given laser excitation source). To verify that the absorbance spectra corresponded to light absorption, rather than scattering, we compared porphysomes with wavelength-matched gold nanorods (with 680 nm extinction peaks) using resonance scattering[21]. Porphysomes exhibited up to 100 times less resonance light scatter at the optical density wavelength peak at which the samples were normalized (Fig. 1d). The monodisperse 100 nm sizes exhibited by various types of porphysome (Fig. 1e) are in a suitable range to take advantage of the enhanced permeability and retention effect for passive accumulation in tumours[22,23]. Flexibility in size control was demonstrated as sonication of porphyrin–lipid in water produced smaller, 30 nm, nanoparticles (Supplementary Fig. S1), which could be useful for applications requiring smaller nanoparticle sizes. Geometric calculations for vesicles of 100 nm

in diameter composed of subunits with phosphatidylcholine headgroups indicate that there are approximately 8×10^4 porphyrin conjugates per porphysome[24]. On the basis of pyropheophorbide absorbance (accounting for differences in the absorbance of the intact porphysome measured in PBS and the dissociated porphyrin–lipid obtained by diluting 1–2 µl of porphysomes in 1 ml of methanol, as shown in Supplementary Fig. S2), we estimate a pyropheophorbide-porphysome extinction coefficient, ε_{680}, of $2.9 \times 10^9\ M^{-1}\ cm^{-1}$. This large, near-infrared extinction coefficient is a reflection of the dense porphyrin packing in the bilayer that generates the unique nanoscale optical behaviour of porphysomes.

To understand the implications of such a high number of porphyrin–lipid conjugates in a 100-nm-diameter nanovesicle, fluorescence self-quenching was examined. As increasing amounts of porphyrin–lipid were included in the formulations of standard liposomes (3:2 molar ratio of egg-yolk phosphatidylcholine/cholesterol), self-quenching increased up to 1,200-fold when porphysomes were formed completely by porphyrin–lipid subunits (Fig. 2a). This is much greater than typical porphyrin quenching[25] and indicates an energetically favourable supramolecular structure in which the porphyrin–lipid orientation facilitates extensive porphyrin interaction and quenching. As PEG–lipid was added to enhance *in vivo* pharmacokinetics, its potential to modulate porphysome self-quenching was assessed. Whereas incorporating 5 molar% distearoylphosphatidylcholine (the lipid portion of the PEG–lipid) did not affect quenching, 5 molar% PEG–lipid modestly enhanced self-quenching to over 1,500-fold (Fig. 2b). This increase was due to the stabilizing effect of PEG, consistent with observations that porphysomes containing PEG maintained their size and monodispersity for at least nine months, whereas those without PEG aggregated rapidly. To assess whether any nanostructure composed of dye–lipid subunits would be sufficient to generate extreme self-quenching, vesicles formed from 7-nitro-2-1, 3-benzoxadiazol-4-yl (NBD)–lipid (a non-ionic dye conjugated to a lipid in a manner similar to that for porphyrin–lipid) were examined. NBD–lipid could not form monodisperse 100 nm vesicles (data not shown) and self-quenching was only 20-fold, highlighting the role of porphyrin interaction in defining porphysome structure and nanoscale properties. Differential scanning calorimetry revealed that the porphyrin–lipid had no apparent transition temperature, indicating that porphyrin stacking is distinct from the typical acyl chain interactions that drive normal lipid transitions in liposomes (Supplementary Fig. S3). To determine whether quenching was solely a characteristic of porphyrin confinement in a bilayer, the behaviour of free porphyrin in liposomes was examined. The maximum amount of free pyropheophorbide that could be incorporated into liposomes was only 15 molar%, because manual extrusion became physically impossible beyond this amount. Porphysomes exhibited five times more self-quenching at corresponding levels of porphyrin–lipid incorporation (Fig. 2a,b), demonstrating again that the porphyrin bilayer structure is essential for extensive self-quenching. Porphyrin-loaded liposomes have been described for biological applications, but can accommodate only a small molar fraction of porphyrin and cannot prevent porphyrin redistribution to serum proteins[26]. Other porphyrin vesicles and diblock co-polymers have been described that incorporate porphyrin subunits, but lower porphyrin density resulted in lower extinction coefficients and an absence of significant fluorescence self-quenching[27,28].

As porphysomes are highly self-quenched, energy that is normally released to fluorescence and singlet-oxygen generation (pyropheophorbide has a combined fluorescence and singlet-oxygen quantum yield approaching unity) is dissipated elsewhere. As seen in Fig. 3a, on exposure to laser irradiation, energy

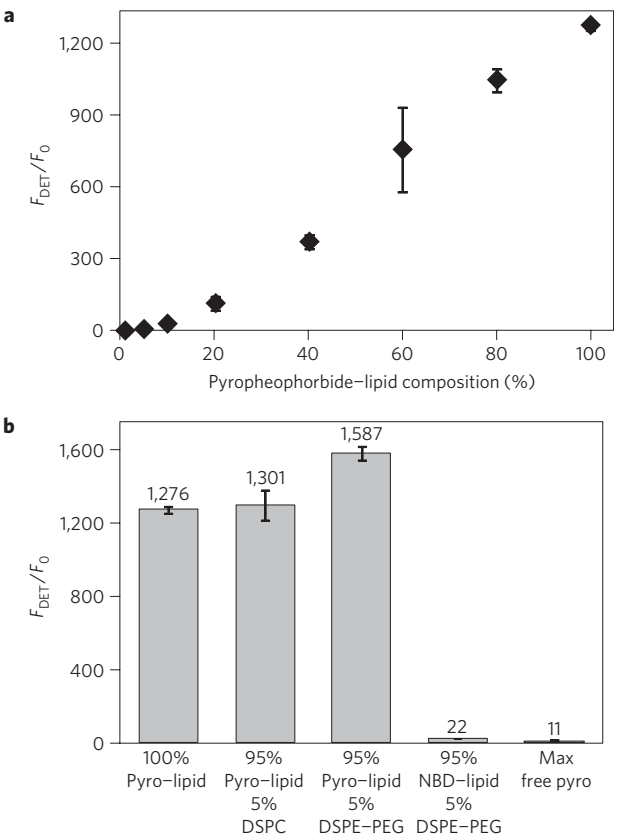

Figure 2 | Porphysomes demonstrate extensive and structurally driven self-quenching. a, Porphysome quenching as a function of molar% pyropheophorbide-lipid (mean ±s.d. from four experiments). The F_{DET}/F_0 values are annotated in the graph. F_0 corresponds to the fluorescence of the porphysomes in PBS and F_{DET} is the fluorescence after disruption of the porphysomes using 0.5% Triton X-100. Nanovesicles were formed from films containing the indicated molar% porphyrin-lipid and the remainder egg-yolk phosphatidylcholine/cholesterol (3:2). **b**, Self-quenching of various nanovesicle formulations (mean ± s.d. from four experiments). DSPC, distearoylphosphatidylcholine; DSPE, distearoylphosphatidylethanolamine. The maximum free porphyrin that could be loaded in liposomes before manual extrusion became physically impossible was 15 molar%.

was released thermally, with an efficiency comparable to gold nanorods (photothermally active inorganic nanoparticles), whereas laser irradiation of standard liposomes generated no significant increase in solution temperature. As photoacoustic signal generation is related to thermal expansion, porphysomes also generated strong photoacoustic signals, proportional to concentration and detectable as low as 25 picomolar, although detection in this range was slightly nonlinear (Supplementary Fig. S4). Although photoacoustic signal is correlated to absorption, when detergent was added to disrupt the porphysome structure (actually generating an increase in absorption), photoacoustic signal decreased up to sixfold (Fig. 3b). The detergent had no effect on the photoacoustic signal of the clinically used contrast agent methylene blue, indicating that the structurally based self-quenching of porphysomes is requisite for nanoscale photoacoustic properties. This basic phenomenon of photoacoustic signal attenuation on detergent-induced porphysome dissociation is demonstrated in the photoacoustic images in Fig. 3c.

We next examined the unique quality that porphysomes are intrinsically suited for both photoacoustic tomography and

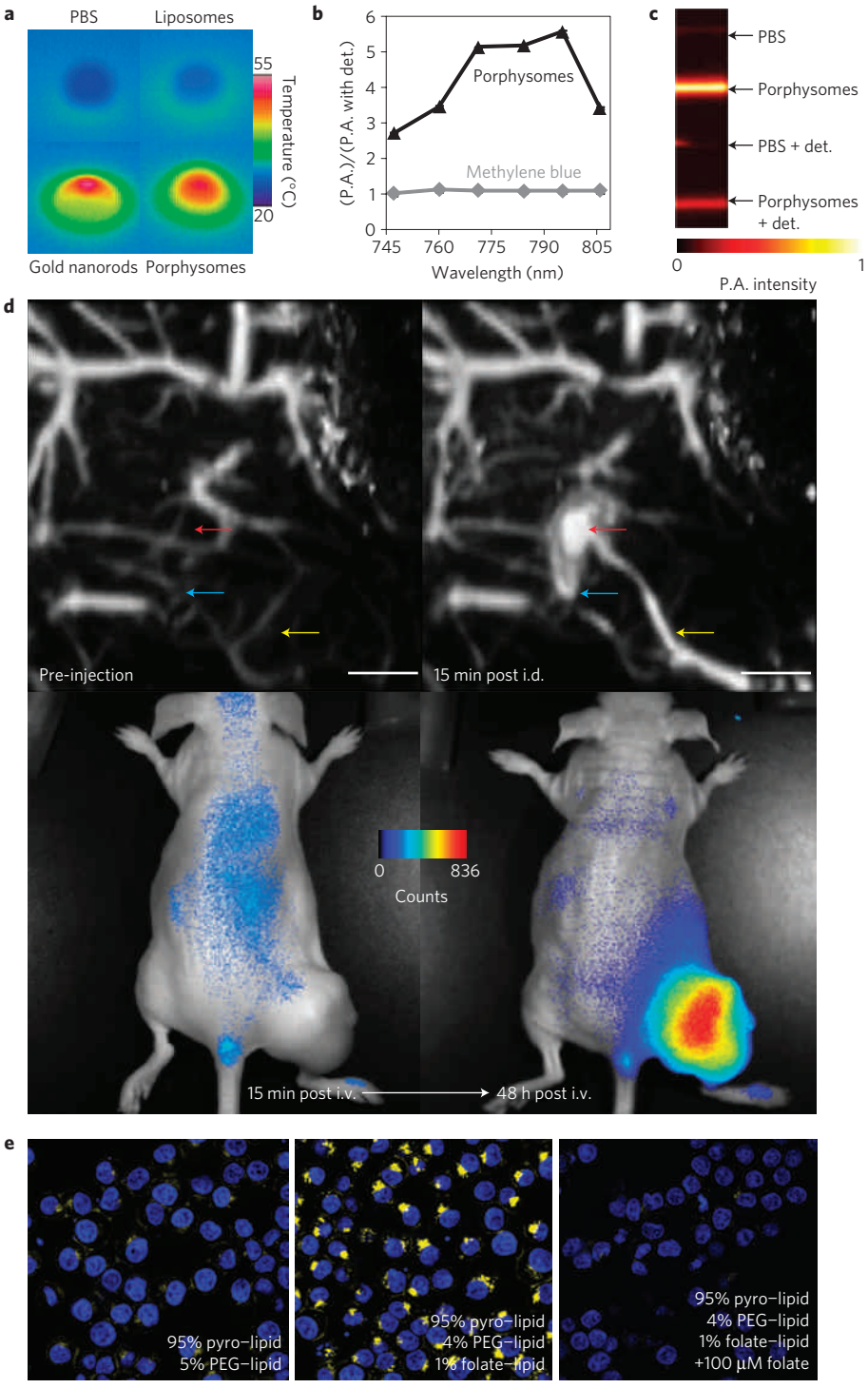

Figure 3 | Multimodal optical utility of porphysomes. a, Photothermal transduction. Solutions were irradiated with a 673 nm laser and imaged with a thermal camera. **b**, Ratio of photoacoustic amplitudes (P.A.) measured for porphysomes and methylene blue ±0.5% Triton X-100 (mean ± s.e.m. from 10 measurements). det., detergent. **c**, Photoacoustic images of tubing containing porphysomes and PBS measured ±0.5% Triton X-100. **d**, Dual modality for photoacoustic contrast and activatable fluorescence. Top, lymphatic mapping. Rats were imaged using photoacoustic tomography before and after intradermal (i.d.) injection of porphysomes (2.3 pmol). Secondary lymph vessels (cyan), lymph node (red), inflowing lymph vessel (yellow) and 5 mm scale bar are indicated. Bottom, fluorescence activation after i.v. injection of porphysomes (7.5 pmol) in a KB xenograft-bearing mouse. **e**, Triggered fluorescence activation on folate-receptor-mediated uptake in KB cells. Porphysomes were incubated for 3 h with KB cells, and porphyrin–lipid (yellow) and nuclei (blue) were visualized with confocal microscopy.

fluorescence imaging *in vivo*. Photoacoustic techniques are gaining recognition and have recently been used to non-invasively detect circulating cancer cells in blood vessels[29], as well as in sentinel lymph nodes[30]. When porphysomes were injected intradermally in rats, the local lymphatic network became clearly detectable within 15 min as porphysomes drained to the lymph vessels and nodes (Fig. 3d, top). Porphysomes exhibited a strong photoacoustic signal, permitting the visualization of the first draining lymph node

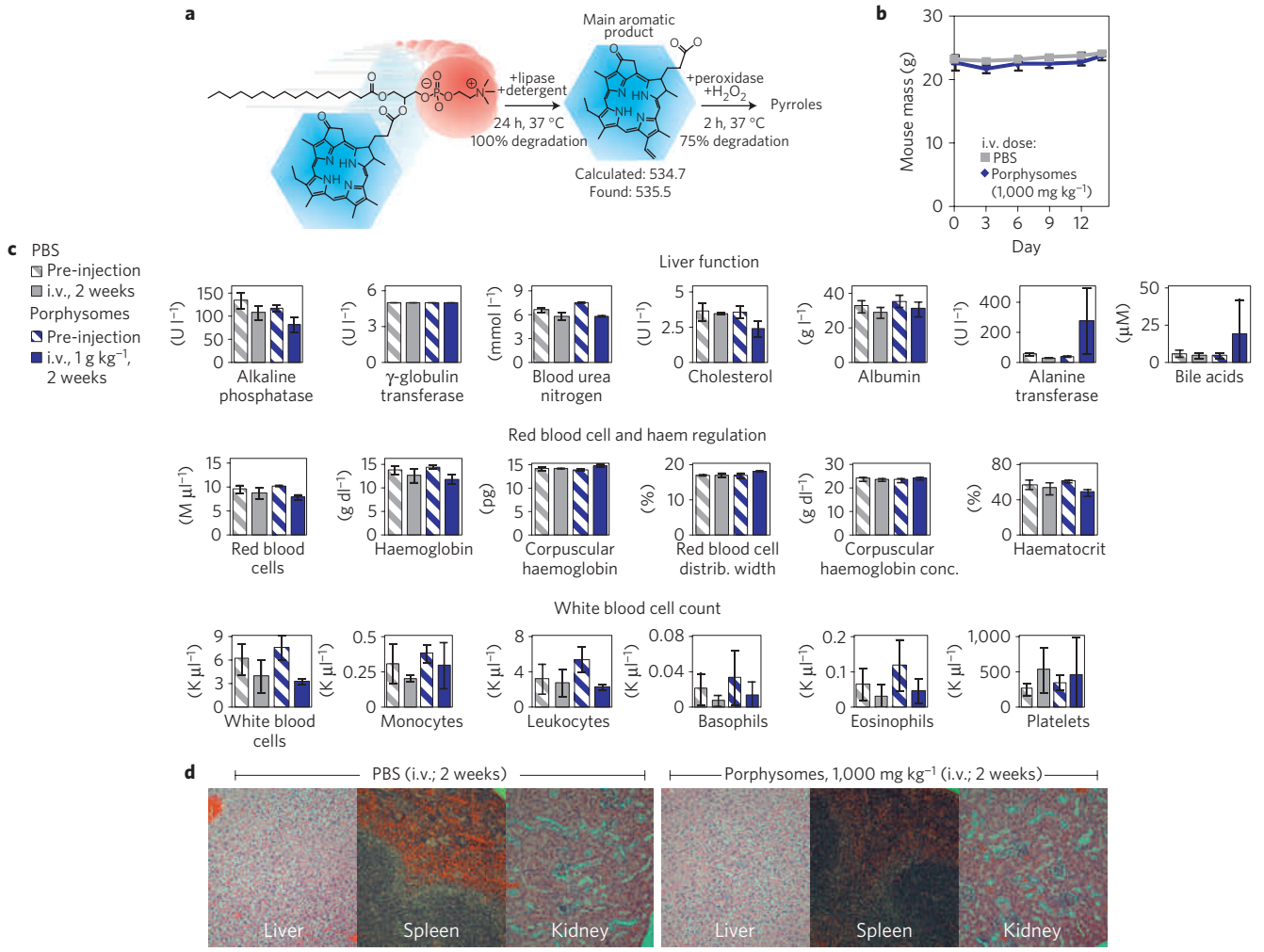

Figure 4 | Porphysomes are enzymatically biodegradable and well tolerated *in vivo*. a, Enzymatic degradation of porphysomes. Porphysomes were lysed with 1% Triton X-100 and incubated with lipase in PBS. Degradation was probed using high-performance liquid chromatography/ mass spectrometry analysis. Purified pyropheophorbide was incubated with peroxidase and degradation was verified by monitoring the loss of absorbance at 680 nm. **b**, Mouse mass change after i.v. administration of 1,000 mg kg^{-1} porphysomes or PBS (mean ± s.d., n = 3). **c**, Blood test parameters for mice with i.v. administration of porphysomes or PBS (mean ± s.d., n = 3). As some test values for γ-globulin transferase results were given as less than 5 U l^{-1}, all values less than 5 U l^{-1} are reported as 5 U l^{-1}. **d**, Representative haematoxylin and eosin stained sections of indicated organs from mice two weeks after i.v. injection of 1,000 mg kg^{-1} porphysomes or PBS.

(red), the inflowing lymph vessel (yellow) and surrounding lymph vessels (cyan). The presence of porphysomes in these lymphatic vessels was directly confirmed by the distinct spectral signature of porphysomes in comparison with that of blood (Supplementary Fig. S5). Other lymph nodes could be traced over time (Supplementary Fig. S6). By using a 6.5 ns pulse width, 10 Hz laser, photoacoustic measurements did not generate sufficient heating to damage surrounding tissues. Next, to investigate whether porphysomes are suited for *in vivo* fluorescence imaging, they were injected intravenously into mice bearing KB cell xenografts. At 15 min post-injection, there was low overall fluorescence signal, demonstrating the self-quenching of porphysomes *in vivo* (Fig. 3d, bottom left). After 2 days, high tumour fluorescence was observed, as porphysomes accumulated in the tumour and became unquenched (Fig. 3d, bottom right), potentially through an enhanced permeability and retention effect or receptor-mediated endocytosis (the porphysomes used for fluorescence imaging included 1 molar% of folate–PEG–lipid). The concept of porphysome quenching *in vivo* was more markedly illustrated when we injected detergent-disrupted porphysomes into mice and observed much higher initial fluorescence (Supplementary Fig. S7). Thus, on the basis of unique self-assembled and nanoscale properties, porphysomes are intrinsically multimodal for both photoacoustic tomography and low background fluorescence imaging. To examine the behaviour of porphysomes on uptake by cancer cells, folate-receptor-targeted porphysomes were produced by including 1 molar% folate–PEG–lipid. The folate receptor is overexpressed in a variety of cancers and effectively internalizes liposomes conjugated to folate[31]. When KB cells (which overexpress the folate receptor) were incubated with folate porphysomes, specific uptake was observed by confocal microscopy and could be inhibited by free folate (Fig. 3e). As intact porphysomes in the incubation media were essentially non-fluorescent, confocal imaging was carried out without a need to change the media. Control experiments revealed that the porphyrin–lipid ended up in endosomes and lysosomes, on the basis of partial co-localization with transferrin and lysotraker (Supplementary Fig. S8).

We next assessed factors relevant to potential clinical applications of porphysomes. To bypass the unknown, long-term side effects of inorganic nanoparticle accumulation in body organs, luminescent silica nanoparticles have been developed that decompose in aqueous solution over a period of hours[32]. Porphysomes

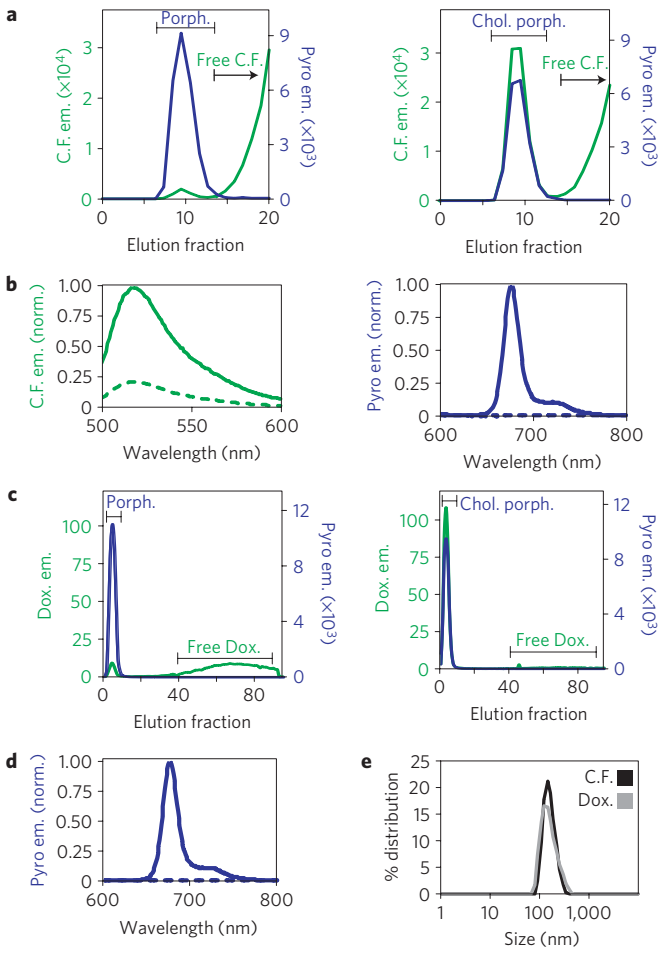

Figure 5 | Active and passive loading of porphysomes. a, Passive loading of carboxyfluorescein (C.F.). Porphysomes composed without (Porph.) or with 30 molar% cholesterol (Chol. porph.) were extruded with 250 mM carboxyfluorescein and gel filtration was carried out. Fluorescence emission (em.) of pyropheophorbide (blue) and carboxyfluorescein (green) was measured in 0.5% Triton X-100 to avoid quenching. **b**, Fluorescence quenching of porphysomes composed with 30 molar% cholesterol (blue) loaded with carboxyfluorescein (green). Spectra were taken before (dashed) and after (solid) addition of detergent and normalized to maximum fluorescence. **c**, Active loading of doxorubicin (Dox.). Fluorescence of gel filtration fractions (collected when porphysomes began to elute) of porphysomes without or with 50 molar% cholesterol. Fluorescence of pyropheophorbide (blue) and doxorubicin (green) was measured with detergent. **d**, Fluorescence quenching of pyropheophorbide in porphysomes composed with 50 molar% cholesterol and loaded with doxorubicin. Normalized spectra were measured before (dashed) and after (solid) addition of detergent. **e**, Size distributions of porphysomes loaded with carboxyfluorescein (black) or doxorubicin (grey).

are stable for months when stored in aqueous solutions, but they were prone to enzymatic degradation (Fig. 4a). On incubation with detergent and lipase, the phospholipid structure was cleaved, with the main aromatic product being pyropheophorbide, which was the starting material in the synthetic reaction generating the porphyrin–lipid. Similarly to chlorophyll, pyropheophorbide is known to be enzymatically cleaved into colourless pyrroles when incubated with peroxidase and hydrogen peroxide[33]. We verified this degradation by monitoring the loss of porphyrin absorption and confirmed that pyropheophorbide could be efficiently degraded by peroxidase. To our knowledge, this is the first example of an enzymatically biodegradable, intrinsically optical active nanoparticle. We next carried out a preliminary study to assess the potential toxicity of porphysomes. When mice were treated with a high dose of porphysomes (1,000 mg kg^{-1}), they remained healthy over a two-week period, as demonstrated by a lack of major behaviour changes or weight loss (Fig. 4b). At the two-week time point, mice were euthanized and blood tests were carried out (Fig. 4c). Liver function tests indicated that the hepatic function of the mice was generally normal, with the exception of elevated levels of bile acids and alanine transferase (less than two times the upper range of normal). Red blood cell counts and attributes were unaffected by the large dose of porphyrin–lipid, which did not interfere with the physiological regulation of endogenous porphyrin (haem). Unaffected white blood cell counts imply that porphysomes were not immunogenic at the two-week time point, even at the high doses given to mice. Post-mortem histopathological examination of the liver, spleen and kidneys indicated that these organs were in good condition and were not impacted by the high intravenous (i.v.) porphysome dose (Fig. 4d).

The large aqueous core of the porphysome, contained within the porphyrin bilayer, has potential for cargo loading (Fig. 1b). When porphysomes (containing 5% PEG–lipid) were hydrated using a 250 mM carboxyfluorescein solution and extruded, only a limited amount of carboxyfluorescein was stably entrapped in the porphysomes, as determined by gel filtration (Fig. 5a, left). As cholesterol is known to enhance loading of compounds within phosphatidylcholine-based liposomes[34], we included 30 molar% cholesterol into the formulation and repeated the passive carboxyfluorescein loading. The cholesterol-containing porphysomes were able to load ~20 times more carboxyfluorescein when compared with the porphysomes lacking cholesterol (Fig. 5a, right). At this high loading concentration, carboxyfluorescein itself was self-quenched in the porphysome (Fig. 5b, left). Furthermore, the porphysome remained fluorescently self-quenched (Fig. 5b, right), indicating that most of the light absorbed by the porphyrin bilayer was converted to heat. As expected, passive loading of carboxyfluorescein entrapped only a small fraction of the total fluorophore in the hydration solution. One of the most powerful drug loading techniques is active loading, which uses pH or ion gradients to concentrate amphipathic weakly basic molecules into liposomes[35] and polymersomes[36]. The importance of this loading technique is reflected by Doxil, the first clinically implemented nanoparticle[37], which is a liposomal formulation of actively loaded doxorubicin. We applied the ammonium sulphate gradient method[35] with a doxorubicin to pyropheophorbide–lipid molar ratio of 1:5 to actively load doxorubicin into porphysomes. Without addition of cholesterol, some loading of doxorubicin was observed by gel filtration, but the fraction of the total doxorubicin incorporated from the solution was approximately 10% (Fig. 5c, left). However, when 50 molar% cholesterol was added to the porphysome formulation, strong active loading was achieved and porphysomes loaded 90% of all free doxorubicin in solution into the porphysome core (Fig. 5c, right). These porphysomes also maintained a self-quenching porphyrin bilayer (Fig. 5d). Both actively and passively loaded porphysomes exhibited monodisperse sizes between 150 nm and 200 nm (Fig. 5e).

Photothermal therapy is an emerging technique that can make use of contrast agents that convert light into heat at target sites. Inorganic nanoparticles including gold nanoshells[14], gold nanorods[38], gold nanocages[39] and graphene[40] have been used to destroy tumours using photothermal therapy. To demonstrate the biophotonic therapeutic potential of an organic nanoparticle, we carried out preliminary experiments using porphysomes as agents for photothermal therapy. We used porphysomes containing 30 molar% cholesterol because they demonstrated favourable

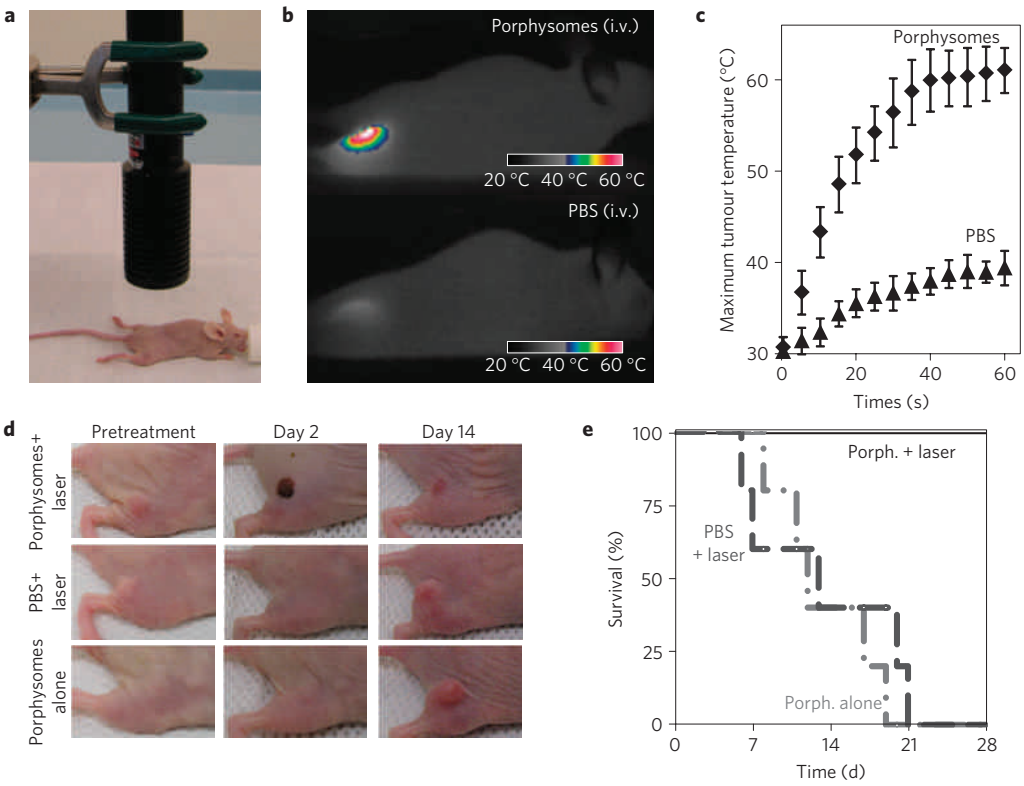

Figure 6 | Porphysomes as photothermal therapy agents. a, Photothermal therapy set-up showing laser and tumour-bearing mouse. **b**, Representative thermal response in KB tumour-bearing mice injected intravenously 24 h before with 42 mg kg^{-1} porphysomes or PBS. Thermal image was obtained after 60 s of laser irradiation (1.9 W cm^{-2}). **c**, Maximum tumour temperature during 60 s laser irradiation (mean ± s.d. for five mice per group). **d**, Photographs showing therapeutic response to photothermal therapy using porphysomes. **e**, Survival plot of tumour-bearing mice treated with the indicated conditions. Mice were euthanized when tumours reached 10 mm in size ($n = 5$ for each group).

biodistribution following systemic administration, with more accumulation in the tumour (3% injected dose per gram) and less accumulation in the liver and spleen than standard porphysomes (Supplementary Fig. S9a). Cholesterol porphysomes also had a 35% longer serum half-life of 8.5 h (Supplementary Fig. S9b). A 658 nm laser outputting 750 mW (with a power density of 1.9 W cm^{-2}) was used to irradiate the KB tumours in xenograft-bearing mice following porphysome administration (Fig. 6a). At 24 h before treatment, mice were injected intravenously with 42 mg kg^{-1} porphysomes or a PBS control. The tumour was then irradiated with the laser for 1 min and temperature was monitored using a thermal camera (Fig. 6b). The tumour temperature in the porphysome group rapidly reached 60 °C, whereas the tumours in mice injected with PBS were limited to 40 °C (Fig. 6c). Following treatment, mice in the porphysome- and laser-treated group developed eschars on the tumours, whereas the laser-alone group and the porphysomes-alone group did not. After two weeks, the eschars healed and the tumours in the treated group were destroyed (Fig. 6d). Unlike the tumours in mice treated with porphysomes and laser treatment, tumours in mice that received laser treatment alone or porphysome injection alone continued to grow rapidly and all of the mice in those groups had to be euthanized within 21 days (Fig. 6e). This photothermal experiment corresponded to a treatment with a therapeutic index of at least 25, given the safety of porphysomes at 1 g kg^{-1} i.v. doses. We believe that porphysomes could impact a range of clinical applications, potentially exploiting synergistic, multimodal optical imaging and therapeutic approaches. However, to achieve clinical relevance, the rapid attenuation of light in biological tissues must be dealt with by leveraging improving light delivery methods or targeting diseases that affect organs that are more accessible to light[41].

Similarly to liposomes, porphysomes are self-assembled from simple monomers, efficient nanocarriers, enzymatically biodegradable and highly biocompatible. A small molar percentage of lipid conjugated to targeting moieties, such as antibodies, aptamers, proteins or small targeting molecules, could be easily incorporated to potentially direct porphysomes to a range of different target cells. Similarly to optically active inorganic nanoparticles, porphysomes have large, tunable extinction coefficients and are effective agents for photothermal and photoacoustic applications. Porphysomes exhibit unique nanoscale optical properties and are intrinsically suited for multimodal imaging and therapeutic applications.

Methods

Formation and characterization of porphysomes. 1-palmitoyl-2-hydroxy-*sn*-glycero-3-phosphocholine (Avanti Polar Lipids) was acylated with the *Spirulina pacifica*-derived pyropheophorbide or *Rhodobacter sphaeroides*-derived bacteriochlorophyll to yield pyropheophorbide–lipid or bacteriochlorophyll–lipid, respectively, as acyl-migrated regioisomers. Porphysomes were formed by dispersion and evaporation of lipids and porphyrin–lipids to form a film. Films were rehydrated with PBS, subjected to freeze–thaw cycles and extruded with a 100 nm polycarbonate membrane at 65 °C. Porphysome size was characterized with a Nanosizer ZS90 (Malvern Instruments). Electron microscopy was carried out with 2% uranyl acetate negative staining and a Tecnai F20 electron microscope (FEI company). Porphysome self-quenching was characterized using a Fluoromax fluorometer (Horiba Jobin Yvon). Porphysome or liposome solutions were excited at 420 nm and emission was measured and integrated from 600 to 750 nm. Background subtraction of an equal concentration of 100 nm egg-yolk phosphatidylcholine/cholesterol (3:2) liposomes was carried out. The fluorescence self-quenching F_{DET}/F_0 of each sample was determined by the ratio of the integrated fluorescence emission in the presence or absence of 0.5% Triton X-100. Resonance light scattering and initial photothermal response were carried out with wavelength-matched gold nanorods (kindly provided by the Kumacheva lab, University of Toronto), adjusted to the same absorbance at 680 nm. For resonance light scattering, excitation and emission were set to the same wavelength and

scanned from 400 to 700 nm. After blank subtraction, the resonance scatter of the two samples was divided. Photothermal response was determined using a thermal camera (Mikroshot) following 60 s of laser irradiation with a 673 nm laser diode outputting 150 mW. Passive loading of porphysomes was accomplished by hydrating the porphyrin–lipid film with 250 mM carboxyfluorescein (Anaspec). Following porphysome preparation, unencapsulated carboxyfluorescein was removed by gel filtration using a PD-10 column (GE Healthcare). To actively load doxorubicin, a 0.45 mg ml^{-1} solution of doxorubicin hydrochloride (Sigma Aldrich) was loaded into porphysomes containing 155 mM ammonium sulphate at pH 5.5 by incubating for 2 h at 37 °C. Free doxorubicin was removed by gel filtration. See Supplementary Information for further details.

Multimodal porphysome imaging and therapy. Photoacoustic measurements were carried out on a photoacoustic system with a Ti:sapphire tunable laser and an ultrasound transducer. The axial and transverse resolutions of the system were 150 μm and 590 μm, respectively. Measurements were carried out at 760 nm using bacteriochlorophyll porphysomes in PBS solution. For structural-dependent studies, the photoacoustic signal of porphysomes was compared with that of porphysomes that had been lysed with 0.5% Triton X-100. Animal experiments involving photoacoustic imaging were carried out in compliance with Washington University guidelines. *In vivo* lymphatic mapping with porphysomes was carried out using Sprague-Dawley rats (~200 g) before and after an intradermal porphysome injection on the left forepaw. Mouse xenograft experiments were carried out in compliance with University Health Network guidelines. For fluorescence imaging, 3×10^6 KB cells were inoculated subcutaneously in nude mice and the xenograft grew for 2–3 weeks. Mice were injected through tail vein with bacteriochlorophyll porphysomes. Imaging was carried out using a Maestro imaging system (CRI) using a 710–760 nm excitation filter and an 800 nm long-pass emission filter. For photothermal therapy, KB tumours were grown in female nude mice by injecting 2×10^6 cells into the right flank of female nude mice. When tumour diameters reached 4–5 mm, 42 mg kg^{-1} of porphysomes containing 30 molar% cholesterol were injected through tail vein. At 24 h post-injection, mice were anesthetized with 2% (v/v) isofluorane and tumours were irradiated with a laser with 750 mW output at 660 nm with a 5 mm by 8 mm spot size. Tumour temperatures were recorded with an infrared camera. Tumour volume was measured daily and mice were euthanized once tumour diameter reached 10 mm. See Supplementary Information for further details.

Porphysome degradation and toxicity. For enzymatic degradation, pyropheophorbide porphysomes were incubated with lipase from *Rhizomucor miehei* (Sigma) for 24 h at 37 °C in PBS containing 0.5% Triton X-100 and 10 mM $CaCl_2$. The solution was then subjected to high-performance liquid chromatography/ mass spectrometry analysis to monitor the generation of the pyropheophorbide starting material. Pyropheophorbide was further degraded according to known procedures[33] by incubating 100 μM pyropheophorbide in 0.25% Triton X-100 with 25 units of horseradish peroxidase type II (Sigma), 250 μM of hydrogen peroxide and 500 μM 2,4-dichlorophenol, and absorption loss at 680 nm was monitored. Toxicity experiments were carried out with six-week-old male BALB/c mice (Charles River) in compliance with University Health Network guidelines. Blood was sampled 6 h before porphysome or saline injection. Blood was subjected to the Mammalian Liver Profile tests (Abaxis), and MASCOT haematology profiling (Drew Scientific) according to the manufacturer's protocol. Mice were injected through tail vein with porphysomes (1,000 mg kg^{-1}) or an equal volume of PBS. Over a two-week period, mice were observed for behavioural changes and weight was monitored. Mice were then killed, after cardiac puncture to obtain blood for analysis and then sent for histopathology analysis. See Supplementary Information for further details.

Received 19 April 2010; accepted 8 February 2011; published online 20 March 2011

References

1. Chan, W. C. W. & Nie, S. Quantum dot bioconjugates for ultrasensitive nonisotopic detection. *Science* **281,** 2016–2018 (1998).
2. Storhoff, J. J., Lucas, A. D., Garimella, V., Bao, Y. P. & Müller, U. R. Homogeneous detection of unamplified genomic DNA sequences based on colorimetric scatter of gold nanoparticle probes. *Nature Biotechnol.* **22,** 883–887 (2004).
3. Dolmans, D. E., Fukumura, D. & Jain, R. K. Photodynamic therapy for cancer. *Nature Rev. Cancer* **3,** 380–387 (2003).
4. O'Neal, D. P., Hirsch, L. R., Halas, N. J., Payne, J. D. & West, J. L. Photo-thermal tumour ablation in mice using near infrared-absorbing nanoparticles. *Cancer Lett.* **209,** 171–176 (2004).
5. Huang, X., El-Sayed, I. H., Qian, W. & El-Sayed, M. A. Cancer cell imaging and photothermal therapy in the near-infrared region by using gold nanorods. *J. Am. Chem. Soc.* **128,** 2115–2120 (2006).
6. Oraevsky, A. A. Laser optoacoustic tomography for medical diagnostics: Principles. *Proc. SPIE* **2676,** 22–31 (1996).
7. Oraevsky, A. A. & Karabutov, A. A. in *Biomedical Photonics Handbook* 2003 edn (ed. Vo-Dinh, T.) 34.1–34.34 (CRC Press, 2003).
8. Xu, M. & Wang, L. V. Photoacoustic imaging in biomedicine. *Rev. Sci. Instrum.* **77,** 041101 (2006).
9. Wang, L. V. Multiscale photoacoustic microscopy and computed tomography. *Nature Photon.* **3,** 503–509 (2009).
10. Vakoc, B. J. *et al.* Three-dimensional microscopy of the tumor microenvironment *in vivo* using optical frequency domain imaging. *Nature Med.* **15,** 1219–1223 (2009).
11. Weissleder, R. & Pittet, M. J. Imaging in the era of molecular oncology. *Nature* **452,** 580–589 (2008).
12. Klostranec, J. M. & Chan, W. Quantum dots in biological and biomedical research: Recent progress and present challenges. *Adv. Mater.* **18,** 1953–1964 (2006).
13. Yguerabide, J. & Yguerabide, E. E. Light-scattering submicroscopic particles as highly fluorescent analogs and their use as tracer labels in clinical and biological applications: I. Theory. *Anal. Biochem.* **262,** 137–156 (1998).
14. Lal, S., Clare, S. E. & Halas, N. J. Nanoshell-enabled photothermal cancer therapy: Impending clinical impact. *Acc. Chem. Res.* **41,** 1842–1851 (2008).
15. Ghosh, P., Han, G., De, M., Kim, C. K. & Rotello, V. M. Gold nanoparticles in delivery applications. *Adv. Drug. Deliv. Rev.* **60,** 1307–1315 (2008).
16. Lewinski, N., Colvin, V. & Drezek, R. Cytotoxicity of nanoparticles. *Small* **4,** 26–49 (2008).
17. Nel, A., Xia, T., Madler, L. & Li, N. Toxic potential of materials at the nanolevel. *Science* **311,** 622–627 (2006).
18. Peer, D. *et al.* Nanocarriers as an emerging platform for cancer therapy. *Nature Nanotech.* **2,** 751–760 (2007).
19. Drain, C. M., Varotto, A. & Radivojevic, I. Self-organized porphyrinic materials. *Chem. Rev.* **109,** 1630–1658 (2009).
20. Harris, J. M. & Chess, R. B. Effect of pegylation on pharmaceuticals. *Nature Rev. Drug Discov.* **2,** 214–221 (2003).
21. Pasternack, R. F. & Collings, P. J. Resonance light scattering: A new technique for studying chromophore aggregation. *Science* **269,** 935–939 (1995).
22. Nagayasu, A., Uchiyama, K. & Kiwada, H. The size of liposomes: A factor which affects their targeting efficiency to tumors and therapeutic activity of liposomal antitumour drugs. *Adv. Drug Deliv. Rev.* **40,** 75–87 (1999).
23. Huang, L., Sullenger, B. & Juliano, R. The role of carrier size in the pharmacodynamics of antisense and siRNA oligonucleotides. *J. Drug Target.* **18,** 567–574 (2010).
24. Hansen, C. B., Kao, G. Y., Moase, E. H., Zalipsky, S. & Allen, T. M. Attachment of antibodies to sterically stabilized liposomes: Evaluation, comparison and optimization of coupling procedures. *Biochim. Biophys. Acta* **1239,** 133–144 (1995).
25. Lovell, J. F., Liu, T. W. B., Chen, J. & Zheng, G. Activatable photosensitizers for imaging and therapy. *Chem. Rev.* **110,** 2839–2857 (2010).
26. Chen, B., Pogue, B. W. & Hasan, T. Liposomal delivery of photosensitising agents. *Expert Opin. Drug Deliv.* **2,** 477–487 (2005).
27. Komatsu, T., Moritake, M., Nakagawa, A. & Tsuchida, E. Self-organized lipid-porphyrin bilayer membranes in vesicular form: Nanostructure, photophysical properties, and dioxygen coordination. *Chem. Eur. J.* **8,** 5469–5480 (2002).
28. Ghoroghchian, P. P. *et al.* Near-infrared-emissive polymersomes: Self-assembled soft matter for *in vivo* optical imaging. *Proc. Natl Acad. Sci. USA* **102,** 2922–2927 (2005).
29. Galanzha, E. I. *et al. In vivo* magnetic enrichment and multiplex photoacoustic detection of circulating tumour cells. *Nature Nanotech.* **4,** 855–860 (2009).
30. Galanzha, E. I. *et al. In vivo* fibre-based multicolor photoacoustic detection and photothermal purging of metastasis in sentinel lymph nodes targeted by nanoparticles. *J. Biophoton.* **2,** 528–539 (2009).
31. Lee, R. J. & Low, P. S. Delivery of liposomes into cultured KB cells via folate receptor-mediated endocytosis. *J. Biol. Chem.* **269,** 3198–3204 (1994).
32. Park, J. *et al.* Biodegradable luminescent porous silicon nanoparticles for *in vivo* applications. *Nature Mater.* **8,** 331–336 (2009).
33. Suzuki, Y., Tanabe, K. & Shioi, Y. Determination of chemical oxidation products of chlorophyll and porphyrin by high-performance liquid chromatography. *J. Chromatogr. A* **839,** 85–91 (1999).
34. Kirby, C., Clarke, J. & Gregoriadis, G. Effect of the cholesterol content of small unilamellar liposomes on their stability *in vivo* and *in vitro*. *Biochem. J.* **186,** 591–598 (1980).
35. Haran, G., Cohen, R., Bar, L. K. & Barenholz, Y. Transmembrane ammonium sulphate gradients in liposomes produce efficient and stable entrapment of amphipathic weak bases. *Biochim. Biophys. Acta* **1151,** 201–215 (1993).
36. Ahmed, F. *et al.* Shrinkage of a rapidly growing tumor by drug-loaded polymersomes: pH-triggered release through copolymer degradation. *Mol. Pharm.* **3,** 340–350 (2006).
37. Heidel, J. D. & Davis, M. E. Clinical developments in nanotechnology for cancer therapy. *Pharm. Res.* **28,** 187–199 (2011).

38. von Maltzahn, G. *et al.* Computationally guided photothermal tumor therapy using long-circulating gold nanorod antennas. *Cancer Res.* **69,** 3892–3900 (2009).
39. Chen, J. *et al.* Gold nanocages as photothermal transducers for cancer treatment. *Small* **6,** 811–817 (2010).
40. Yang, K. *et al.* Graphene in mice: Ultrahigh *in vivo* tumor uptake and efficient photothermal therapy. *Nano Lett.* **10,** 3318–3323 (2010).
41. Wilson, B. C. & Patterson, M. S. The physics, biophysics and technology of photodynamic therapy. *Phys. Med. Biol.* **53,** R61–R109 (2008).

Acknowledgements

We thank B. G. Neel for editing, B. C. Wilson and C. M. Yip for insightful discussion, P. V. Turner for histopathology analysis, and E. Kumacheva and L. Tzadu for providing gold nanorods. This work was supported by grants from the Ontario Institute for Cancer Research, the Canadian Cancer Society, the Natural Sciences and Engineering Research Council of Canada, the Canadian Institute of Health Research, the Canadian Foundation of Innovation, the Joey and Toby Tanenbaum/Brazilian Ball Chair in Prostate Cancer Research, and in part from the Campbell Family Institute for Cancer Research, the Princess Margaret Hospital Foundation and the Ministry of Health and Long-Term Planning.

Author contributions

J.F.L. and G.Z. conceived the project, interpreted the data and wrote the manuscript. J.F.L., W.C.W.C. and G.Z. planned the experiments. C.S.J. and J.F.L. carried out photothermal tumour ablation. C.S.J. carried out confocal microscopy. E.H. and J.F.L. carried out most porphysome formation, photophysical characterization and drug encapsulation. H.J. and J.F.L. carried out toxicity experiments. J.L.R. carried out electron microscopy. C.K and L.V.W. carried out the photoacoustic experiments. W.C. and J.F.L. prepared the porphysome starting materials.

Additional information

The authors declare no competing financial interests. Supplementary information accompanies this paper on www.nature.com/naturematerials. Reprints and permissions information is available online at http://npg.nature.com/reprintsandpermissions. Correspondence and requests for materials should be addressed to G.Z.